SEMARAK ILMU PUBLISHING

CFD Letters

Journal homepage:
https://semarakilmu.com.my/journals/index.php/CFD_Letters/index
ISSN: 2180-1363

Numerical Analysis of Blood Flow Behaviour in a Constricted Porous Bifurcated Artery under the Influence of Magnetic Field

Norliza Mohd Zain[1], Zuhaila Ismail[1,*], Peter Johnston[2]

[1] Department of Mathematical Sciences, Fakulti of Science, Universiti Teknologi Malaysia, 81310 Johor Bahru, Johor, Malaysia
[2] Technology Building (N44), School of Environment and Science, Griffith University, Nathan, 4111 Queensland, Australia

ARTICLE INFO

Article history:
Received 11 August 2022
Received in revised form 8 October 2022
Accepted 22 November 2022
Available online 11 January 2023

Keywords:

Galerkin least-squares; non-Newtonian; Bifurcated artery; Overlapping stenosis; Magnetohydrodynamics; Porosity

ABSTRACT

A numerical investigation concerning the effect of arterial constriction on the flow behaviour of blood in a porous bifurcated artery under the influence of a transverse magnetic field has been carried out. The equations of motion governing the flow are derived in the Cartesian coordinate system by treating the fluid as an electrically conducting, Newtonian, incompressible and fully developed blood flow. The blood is considered to flow through a constricted bifurcated artery with overlapping stenosis located at the mother artery. This developed model is consistent with the principles of magnetohydrodynamics. A stabilized form of finite element method, known as the Galerkin least-squares method is employed in solving the governing equation with suitably prescribed boundary conditions. Then, the non-linear systems resulting from the developed model are linearized by an iterative technique called the Newton-Raphson method. The effects of various parameters particularly the severity of stenosis, magnetohydrodynamics constant and permeability parameter on blood flow characteristics are analysed graphically for the velocity profile and streamline pattern. The findings obtained show that the presence of a magnetic field caused a significant alteration in the blood flow behaviour. Slight changes occurred in the flow pattern with the porous medium consideration. The application of a magnetic field could be utilized in controlling the hemodynamic flow of blood by decelerating the flow velocity and reducing the vortex sizes with rising in Hartmann number. While the pathological state of arterial disease as a porous structure reveals that a more porous fluid medium could have slightly promoted the growth in vortex size.

1. Introduction

Haemodynamic modelling of blood circulation in human arteries has received much attention among researchers and become one of the popular areas in scientific research of feasible medical and engineering applications. This matter was encouraged by the growing numbers of mortality and morbidity that resulted from progressive vascular diseases, such as hypotension, hypertension, heart attack and stroke that have occurred in most developed countries [1]. A blockage that is developed at the arterial lumen due to the deposition of atherosclerotic plaque is made up of fatty substances,

* *Corresponding author.*
E-mail address: zuhaila@utm.my

https://doi.org/10.37934/cfdl.15.1.3958

calcium, fibrin, cellular waste and cholesterol [2,3]. The built-up of this deposition which is medically known as stenosis is also a leading cause to many cardiovascular diseases [1,3]. The presence of this constriction leads to a lack of blood supply to the other tissues and organs [4], where the blood has to pass through the narrowed artery at relatively high pressure [1]. As the plaque built up gets hardened and narrowed down the arterial lumen, blood supply to tissue and organ then may reduce or completely block, where these worse conditions may eventually contribute to necrosis as well as strokes [1,2]. This severe disability happens as a result of permanent damage that has occurred to cells in the organ due to an insufficient amount of blood received [4]. It has been reported in numerous studies that the development of stenotic artery certainly disturbs the nature of blood movement and contributes to serious detrimental effects on individual health. The pathological states of a diseased vessel as a porous structure should be taken seriously considering that stenosis is developed by the deposition of fatty substances and the proliferation of connective tissues on the endothelium [3-7]. Due to that, the geometry of stenosis has been modelled in previous works of literature by using various kinds of shapes to portray them close to its pathological condition. Stenosis can be categorized as single or multiple type stenosis. The cosine shaped [8], mild shaped [9], composite shaped [10] and bell shaped [11] can be classified as single stenosis. Whereas, overlapping shaped stenosis is categorized as multiple stenoses. Stenosis may develop anywhere in more than one place, however, arteries with curvatures, junctions and bifurcations are sites that are prone to atherosclerotic plaque development [6]. In medical, patients are usually diagnosed with multiple types of stenosis which favourably develop at the femoral and pulmonary arteries [12].

Blood is composed of 45% formed elements comprising the living cells of erythrocytes (red blood cells), leukocytes (white blood cells) and platelets which are suspended in the plasma [4]. Due to that, blood is also known as a fluid connective tissue. Since erythrocytes contain haemoglobin that is rich in iron protein and these cells are the major components of the haematocrit, hence, an application of a magnetic field may have altered the movements of blood [6]. Blood exhibits an electrical conductivity property that when subjected to an external magnetic field will produce a body force known as Lorentz force [4]. The interaction between the induced electric current on the erythrocytes and an externally applied magnetic field tends to orient the cells along its long axis in the direction of the magnetic field [5]. Exposure to an externally applied magnetic field caused an opposing motion to the blood flow due to the anisotropic orientation of erythrocytes which may also enhance the viscosity of blood [5]. This working principle is in line with the magnetohydrodynamics (MHD) principle and has been widely implemented in medical engineering. For instance, the principles are being utilized for the treatments of haemorrhages, gastric infections and hypertension, also to regulate bleeding during surgeries and provocation of occlusion of the feeding vessels for the cancer tumours [6]. The rheological behaviour of blood flowing through a large artery is valid to be treated as a Newtonian model [13]. However, the fact that the blood flow through a diseased vessel exhibits a low shear flow that shows a prominent characteristic of blood as a non-Newtonian fluid could not be ignored. Besides, the study on porosity effects on the blood flow should be taken seriously since most of the natural flows are related to the porous medium.

The effects of an applied magnetic field and multiple stenoses on a non-Newtonian model of blood flow were investigated by Varshney *et al.* [12]. Jain *et al.* [3] examined analytically the influences of porosity constant and magnetic number on the Newtonian model of blood flow through an artery with a cosine shaped stenosis. Sinha *et al.* [7] analytically explored the effects of a transverse magnetic field and porous medium on the Newtonian model of blood flow in terms of stream function, flow velocity as well as wall shear stress. A mathematical model of the Newtonian model of blood flow through a porous vessel with a pair of stenosis subjected to the ferrohydrodynamics (FHD) and magnetohydrodynamics (MHD) principles was developed in [5].

Misra *et al.*[5] solved the study analytically where they discovered the worsening effects of the magnetic field on the wall shear stress if an over-amplified intensity is applied externally, which can lead to the occurrence of plaque rupture. The effects of slip permeable wall and body acceleration through a constricted porous artery subjected to an externally applied magnetic field were examined by Nandal *et al.* [1]. They concluded with an appropriate strength of magnetic field exposure, the excessive amount of blood pressure on the heart could be overcome. Hence, this finding would be beneficial for the treatment of necrosis, joint pain, muscle pain, travel sickness and headaches [1]. In analytical work done by Srivastava [2], the role of porosity subjected to the MHD effects was studied by considering an inclined tapered artery with mild stenosis under the influence of an inclined magnetic field. The mathematical analysis carried out in their study discovered similar behaviours of blood when subjected to an external magnetic field with a porous medium effect as the one presented in the previous study highlighted in [1], [3], [5] and [7]. The axial velocity distributions were observed to have a respective enhancing and diminishing effect on the permeability of the porous vessel and magnetic field applied externally. While transferring blood to body tissues, molecules of various sizes can either penetrate or pass the lumen of the endothelial cells as they contain ultra-macroscopic pores which indicates the permeability of the vessels [7]. Hence, the pathological conditions of the human vessel as a porous medium are one of the essential hydrodynamic properties that should be considered in understanding blood flow in the entire circulatory system. The aforementioned works were all considered arterial constriction on a straight vessel. There is very limited study considered a blockage in the bifurcated artery, despite its huge propensity of being site favourably predisposed to atherosclerotic plaque development. The physical features of branch arteries which contained curvatures, bifurcations and junctions make them more feasible to flow disturbances that usually developed here where plaques are frequently formed [13]. The study on the behaviour of blood flow in a diseased bifurcated artery has been investigated in [13], [14] and [15]. However, none of this study considered a porous medium and magnetic field effects.

Keeping in view of the motivation as specified above, further investigation needs to be carried out to gain a better insight into the actual interactions between an external magnetic field application and the pathological condition of the blood vessel as a porous medium with the rheological behaviours of the streaming blood in a diseased vessel of a bifurcated artery. Findings from this study would be beneficial for the pathologists and medical scientists for them to analyse and understand the influence of magnetic fields on human blood circulation while receiving magnetic medical therapies. The effects of this localized plaque on the flow structure of blood in the mother and daughter artery will be examined in terms of the axial flow velocity and streamline pattern. The flow of blood through a stenosed bifurcated artery which possessed overlapping shaped stenosis in the mother artery is treated as a Newtonian fluid model by using a Cartesian coordinate system in two-dimensional. The resulted governing equations with appropriate boundary conditions for the specified problem under consideration will be solved by using the stabilized form of the finite element method (FEM), namely the Galerkin least-squares (GLS) method. This method is developed to enhance the stability of the classical Galerkin method due to various numerical instabilities that have emerged to achieve a compatible combination for the velocity and pressure subspaces [16]. With this method, the Babuška-Brezzi stability condition can be neglected and equal order of interpolation functions for velocity and pressure components could be employed. The efficiency of this method in solving incompressible shear flows was discussed in [17-20]. To deal with the nonlinearity arising from the developed systems, the Newton-Raphson method is employed where the numerical integrals are evaluated by using the Gaussian quadrature technique.

2. Problem Formulation

2.1 Governing Equations

Let us consider a steady, laminar, incompressible, electrically conducting fluid and Newtonian in nature flow of blood through a porous medium in a stenosed bifurcated artery having single overlapping stenosis at the mother artery under the influence of an externally applied magnetic field in a transverse direction. The magnetic Reynolds number is assumed to be very small, hence, the induced magnetic field is negligibly small in comparison to the applied magnetic field. This indicates that the flow of blood has a very small value of electrical conductivity. The assumptions considered here are applicable for a situation when human body is subjected to an external magnetic field, for instance when patients undergo the electromagnetic therapy for the treatment of tumor or cancer [7], and while performing the magnetic resonance imaging (MRI) for medical examinations. Since stenosis might develop on the endothelium through the proliferation of connective tissues and by the deposition of fatty substances and cholesterol [7], hence such pathological states is described in this study by considering the flow of blood through a porous structure of a diseased vessel. Meanwhile, the arterial constriction is portrayed here as an overlapping shaped stenosis which can be classified as a multiple stenosis that is commonly found in most medical situations located at femoral and pulmonary arteries [12]. The assumption of wall rigidity considered here is reasonable for a diseased vessel considering that the artery is less compliant, thus reducing the wall motion [21]. This is resulted from the high level of cholesterol in blood that leads to the accumulation of fat on the inner wall of an artery, which later might stimulate the hardening of the artery [22]. This matter caused the malfunction of endothelial cells, thus reducing the lumen capability [23]. Under the specified assumptions of the physiological relevance, the equations of motions governing such fluid flows in vector form are the continuity and momentum as follows,

$$\begin{aligned} &\nabla\cdot\bar{\mathbf{u}}=0 && \text{in } \bar{\Omega},\\ &\rho\bar{\mathbf{u}}\cdot\nabla\bar{\mathbf{u}}-\nabla\cdot\left(2\eta(\dot{\gamma})\mathbf{D}\right)+\nabla\bar{p}=\rho\bar{\mathbf{f}} && \text{in } \bar{\Omega}, \end{aligned} \tag{1}$$

where $\bar{\mathbf{u}}$ is the velocity component, ρ is the density of blood, $\eta(\dot{\gamma})$ is the viscosity function, $\bar{p}$ is the pressure or volumetric stress, $\bar{\mathbf{f}}$ is the dimensional body force vector and $\bar{\Omega}$ represents the dimensional form domain. Due to the unidirectional flow assumption of velocity which flows through in an axial direction, the body force vector $\bar{\mathbf{f}}$ can be defined as the electromagnetic force specified as $-\sigma B_0^2\bar{u}$ for the MHD flow which appears in $x-$momentum equation. This term represents the Lorentz force per unit volume and arises due to the electrical conductivity of blood, σ which is considered as 0.8Sm^{-1} by neglecting the dependence of electrical conductivity with the temperature [24]. The parameter B_o indicates the magnetic flux intensity which acts in a direction perpendicularly to the flow of blood. Meanwhile, the terms $-\frac{\mu}{k}\bar{u}$ and $-\frac{\mu}{k}\bar{v}$ acts as the body force vector $\bar{\mathbf{f}}$ which appear respectively in x and $y-$momentum equations as the pathological state of blood as a porous medium. The viscosity function $\eta(\dot{\gamma})$ in Eq. (1) is treated as a constant viscosity that describe the Newtonian fluid, which is indicated by the parameter μ. While, k is a constant that define the permeability of the porous medium. Given that, the corresponding Eq. (1) are written in a two-dimensional Cartesian coordinate system as,

$$\frac{\partial \bar{u}}{\partial \bar{x}}+\frac{\partial \bar{v}}{\partial \bar{y}}=0,$$
$$\rho\left[\frac{\partial \bar{u}}{\partial \bar{x}}+\frac{\partial \bar{u}}{\partial \bar{y}}\right]=-\frac{\partial \bar{p}}{\partial \bar{x}}+\mu\left[\frac{\partial^2 \bar{u}}{\partial \bar{x}^2}+\frac{\partial^2 \bar{u}}{\partial \bar{y}^2}\right]-\sigma B_0^2 \bar{u}-\frac{\mu}{k}\bar{u}, \tag{2}$$
$$\rho\left[\frac{\partial \bar{v}}{\partial \bar{x}}+\frac{\partial \bar{v}}{\partial \bar{y}}\right]=-\frac{\partial \bar{p}}{\partial \bar{y}}+\mu\left[\frac{\partial^2 \bar{v}}{\partial \bar{x}^2}+\frac{\partial^2 \bar{v}}{\partial \bar{y}^2}\right]-\frac{\mu}{k}\bar{v}.$$

2.2 Boundary Conditions

The system of equations specified in Eq. (2) is solved for the velocity and pressure components given the appropriate boundary conditions. The associated boundary conditions for the problem under consideration are,

$$\bar{u}=\bar{u}_{\max}\left(1-\left(\frac{\bar{y}}{\bar{h}}\right)^2\right) \text{ and } \bar{v}=0, \text{ on } \bar{\Gamma}_{inlet}, \tag{3}$$

corresponding to the Dirichlet boundary condition being prescribed at the flow entrance where the characteristic length $\bar{h}$ refers to the length of the arterial inlet, $\bar{\Gamma}_{inlet}$ is the inlet boundary of the domain $\bar{\Omega}$ and $\bar{u}_{\max}$ represents the maximum inflow velocity. Meanwhile, along the wall boundary $\bar{\Gamma}_{wall}$ of the rigid vessel, a non-slip condition is assumed to take place as follows,

$$\bar{u}=0 \text{ and } \bar{v}=0, \text{ on } \bar{\Gamma}_{wall}. \tag{4}$$

At the outlet boundary $\bar{\Gamma}_{outlet}$, a traction-free condition is being imposed. This Neumann boundary condition can be written mathematically as,

$$\left(-\bar{p}\mathbf{I}+2\mu\mathbf{D}\right)\mathbf{n}=\mathbf{t}_h, \text{ on } \bar{\Gamma}_{outlet}, \tag{5}$$

where $\mathbf{n}$ is the unit outward normal vector, $\mathbf{t}_h$ is a vector of the prescribed boundary tractions, $\mathbf{I}$ is the unit tensor, and $\mathbf{D}$ is the strain rate tensor which may be defined as

$$\mathbf{D}=\frac{1}{2}\left(\nabla\bar{\mathbf{u}}+\left(\nabla\bar{\mathbf{u}}\right)^T\right). \tag{6}$$

2.3 Computational Domain – Stenosed Bifurcated Artery

The schematic diagram for the stenosed bifurcated artery considered in this study is illustrated in Figure 1. To ease the interpretation of the geometry, Figure 1 is portrayed in a non-dimensionalised form where the units for each parameter involved in constructing the geometry are being normalised by dividing them by the characteristic length, $\bar{h}$ value. The computational domain considered here is adopted from the study conducted by Chakravarty *et al.* [20] and Chakravarty *et al.* [25] for the respective construction of bifurcated channel and arterial constriction. Let $\bar{x}$ and $\bar{y}$ be the Cartesian coordinate system of a material point where the x-axis is taken along the axis of the trunk, while the

y-axis is taken along the radial direction. The geometry of the diseased blood vessel is developed mathematically from equations describing the radii of the outer and inner wall, respectively as $\overline{R}_1\left(\overline{x}\right)$ and $\overline{R}_2\left(\overline{x}\right)$ as follows,

$$\overline{R}_1\left(\overline{x}\right)=\begin{cases} a, & 0\le \overline{x}\le d \text{ and } d+l_0\le \overline{x}\le x_1,\\ a-\dfrac{3\tau_m}{2l_0^{\,4}}\left\{\begin{matrix}11\left(x-d\right)l_0^3-47\left(x-d\right)^2 l_0^2\\ +72\left(x-d\right)^3 l_0-36\left(x-d\right)^4\end{matrix}\right\}, & d\le \overline{x}\le d+l_0,\\ a+r_0-\sqrt{r_0^2-\left(x-x_1\right)^2}, & x_1\le \overline{x}\le x_2,\\ 2r_1\sec\beta+\left(x-x_2\right)\tan\beta, & x_2\le \overline{x}\le x_{\max}-s. \end{cases} \tag{7}$$

$$\overline{R}_2\left(\overline{x}\right)=\begin{cases} 0, & 0\le \overline{x}\le x_3,\\ \sqrt{r_0^{'}-\left(x-\left(x_3+r_0^{'}\right)\right)^2}, & x_3\le \overline{x}\le x_4,\\ r_0^{'}\cos\beta+\left(x-x_4\right)\tan\beta, & x_4\le \overline{x}\le x_{\max}, \end{cases} \tag{8}$$

where a and r_1 represent the respective radii for the mother and daughter artery. r_0 and $r_0^{'}$ indicate the radii of curvature for the lateral junction and the flow divider, respectively. Whereas, l_0 is the length of the stenosis at a distance d from the origin. Location of the onset and offset of the lateral junction are respectively denoted as x_1 and x_2. The apex of the vessel is characterized by x_3. τ_m represents the maximum height of stenosis which occurred at two different locations of $d+2l_0/6$ and $d+4l_0/6$. While, β acts as half of the bifurcation angle. Parameters involved in Eqs. (7) and (8) are defined as

$$\begin{aligned} &x_2=x_1+r_0\sin\beta, r_0=\frac{a-2r_1\sec\beta}{\cos\beta-1},\ r_0^{'}=\frac{\left(x_3-x_2\right)\sin\beta}{1-\sin\beta},\\ &x_3=x_2+q,\ s=2r_1\sin\beta,\ x_4=x_3+r_0^{'}\left(1-\sin\beta\right), \end{aligned} \tag{9}$$

where q is a small number that lies in the range of $0.0001\le q\le 0.0005$ that is chosen according to the compatibility of the geometry. Besides that, the following assumptions are imposed on our model,

i. The artery forming bifurcation is of finite length.
ii. The parent aorta possesses a single overlapping shaped stenosis in its lumen and is symmetrical about the axis of the vessel.
iii. Curvatures are introduced at the lateral junctions and the flow divider of the arterial bifurcation to ensure that one can rule out the presence of any discontinuity causing non-existent separation zones.
iv. The constricted artery is considered equivalent to fictitious porous medium.

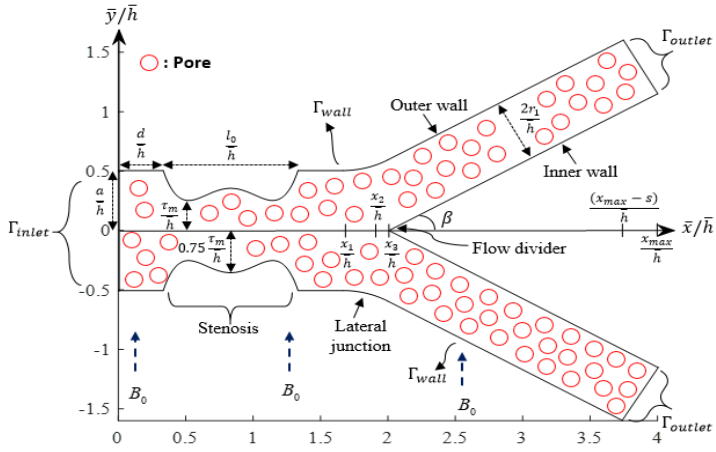

Fig. 1. Schematic diagram for the geometry of stenosed porous bifurcated artery with magnetic flux intensity, B_0 acts perpendicularly to the flow direction

3. Solution Procedure

3.1 Non-dimensionalisation of Equations

To obtain the governing equations and boundary conditions in non-dimensional form, these following non-dimensional variables are introduced as

$$x=\frac{\bar{x}}{\bar{h}},\ y=\frac{\bar{y}}{\bar{h}},\ u=\frac{\bar{u}}{\bar{u}_r},\ v=\frac{\bar{v}}{\bar{u}_r},\ p=\frac{\bar{p}}{\rho\bar{u}_r^2}, \tag{10}$$

where, the characteristic length, $\bar{h}$ refer to the length of the channel's inlet. While, the reference velocity, $\bar{u}_r$ represents the average mean inflow velocity. By the substitution of these non-dimensional variables in Eq. (10) to system of governing equations described in Eq. (2), the simplified form of Eq. (2) is obtained as,

$$\begin{aligned}
&\frac{\partial u}{\partial x}+\frac{\partial v}{\partial y}=0,\\
&\frac{\partial u}{\partial x}+\frac{\partial u}{\partial y}=-\frac{\partial p}{\partial x}+\frac{1}{\mathrm{Re}}\left[\frac{\partial^2 u}{\partial x^2}+\frac{\partial^2 u}{\partial y^2}\right]-\frac{M^2}{\mathrm{Re}}u-\frac{1}{\mathrm{Re}\cdot K}u,\\
&\frac{\partial v}{\partial x}+\frac{\partial v}{\partial y}=-\frac{\partial p}{\partial y}+\frac{1}{\mathrm{Re}}\left[\frac{\partial^2 v}{\partial x^2}+\frac{\partial^2 v}{\partial y^2}\right]-\frac{1}{\mathrm{Re}\cdot K}v.
\end{aligned} \tag{11}$$

where Re, M and K are the Reynolds number, Hartmann number, and porosity permeability parameter that appear, respectively as the bar is being dropped from the system and they can be defined as,

$$\mathrm{Re}=\frac{\rho\bar{u}_r\bar{h}}{\mu},\ M=B_o\left(\frac{\sigma\bar{h}^2}{\mu}\right)^{1/2}\ \text{and}\ K=\frac{k}{\bar{h}^2}. \tag{12}$$

The boundary conditions specified in Eqs. (3)-(5) are also transformed to their respective dimensionless forms,

$$\begin{aligned} &u = \frac{3}{2}\left(1 - \left(\frac{y}{0.5}\right)^2\right) \text{ and } v = 0, \text{ on } \Gamma_{inlet}, \\ &u = 0 \text{ and } v = 0, \text{ on } \Gamma_{wall}, \\ &(-p\mathbf{I} + \frac{1}{\mathrm{Re}}\mathbf{D})\mathbf{n} = \mathbf{t}_h, \text{ on } \Gamma_{outlet}. \end{aligned} \tag{13}$$

Besides, by using the transformation variables introduced in Eq. (10), the boundary configuration of the computational domain constructed from Eqs. (7) and (8) has been non-dimensionalised to a horizontal length of 4 with their vertical inlet equal to 1 as shown in Figure 1.

To simplify the implementation of GLS method which will be discussed further in the next sub-section, the non-dimensional form of governing equations in (11) with the employed boundary conditions in (13) are written in their vector forms as follow,

$$\begin{aligned} &\nabla \cdot \mathbf{u} = 0 && \text{in } \Omega, \\ &\mathbf{u} \cdot \nabla \mathbf{u} - \frac{1}{\mathrm{Re}} \nabla \cdot \mathbf{D} + \nabla p = \mathbf{f} && \text{in } \Omega, \\ &\mathbf{u} = \mathbf{u}_g && \text{on } \Gamma_g, \\ &(-p\mathbf{I} + \frac{1}{\mathrm{Re}}\mathbf{D})\mathbf{n} = \mathbf{t}_h, && \text{on } \Gamma_{outlet}, \end{aligned} \tag{14}$$

where Γ_g denotes part of the boundary Γ of the domain Ω where Dirichlet boundary conditions are being imposed.

3.2 Galerkin Least-squares Algorithms

The appropriate spaces for the approximations of the velocity $(\mathbf{V}_h)$ and pressure fields (P_h) are defined according to the usual finite element subspaces in fluid dynamics [18] and [19] given as

$$\begin{aligned} &\mathbf{V}_h = \left\{\mathbf{N} \in H_0^1(\Omega)^N \mid \mathbf{N}_{|\mathrm{K}} \in R_k(\Omega_K)^N, \Omega_K \in C_h\right\}, \\ &P_h = \left\{p \in C^0(\Omega) \cap L_0^2(\Omega) \mid p_{|\mathrm{K}} \in R_l(\Omega_K), \Omega_K \in C_h\right\}. \end{aligned} \tag{15}$$

The parameters R_k and R_l in Eq. (15) represent the polynomial spaces of degrees k and l, respectively defined over a finite element partition, C_h of the problem domain $\overline{\Omega}$ consisting of a triangular element $P_m(\Omega_K)$ parametrized by characteristic mesh size, h_K. The number of space dimensions, N is equal to 2. Unlike in the standard Galerkin method, any combination of integers is allowed for k and l in the GLS method, hence, these two parameters are defined here as 2 corresponding to the quadratic triangular element $P_2(\Omega_K)$ used to discretise the computational domain.

Based on the approximation functions defined in Eq. (15), a Galerkin least-squares formulation considered in this study can be stated as to find $\mathbf{u}_h \in \mathbf{V}_h$ and $p_h \in P_h$ such that,

$$B(\mathbf{u}_h, p_h; \mathbf{N}, q) = F(\mathbf{N}, q),\ \forall (\mathbf{N}, q) \in (\mathbf{V}_h \times P_h), \tag{16}$$

where,

$$\begin{aligned} B(\mathbf{u}, p; \mathbf{N}, q) &= \int_\Omega \mathbf{u} \cdot \nabla \mathbf{u} \cdot \mathbf{N} d\Omega + \int_\Omega \frac{1}{\mathrm{Re}} \mathbf{D}(\mathbf{u}) \cdot \mathbf{D}(\mathbf{N}) d\Omega - \int_\Omega p \nabla \cdot \mathbf{N} d\Omega \\ &- \int_\Omega q \nabla \cdot \mathbf{u} d\Omega + \sum_{\Omega_{K \in C_h}} \int_{\Omega_K} \left[\begin{array}{c} \left(\mathbf{u} \cdot \nabla \mathbf{u} + \nabla p - \nabla \cdot \left(\frac{1}{\mathrm{Re}} \mathbf{D}(\mathbf{u}) \right) \right) \\ \cdot \left(\tau(\mathrm{Re}_K) \right) \left(\mathbf{u} \cdot \nabla \mathbf{N} - \nabla q - \nabla \cdot \left(\frac{1}{\mathrm{Re}} \mathbf{D}(\mathbf{N}) \right) \right) \end{array} \right] d\Omega_K, \\ F(\mathbf{N}, q) &= \int_\Omega \mathbf{f} \cdot \mathbf{N} d\Omega + \int_\Gamma \mathbf{t}_h \cdot \mathbf{N} d\Gamma \\ &+ \sum_{\Omega_{K \in C_h}} \int_{\Omega_K} \left[\mathbf{f} \cdot \left(\tau(\mathrm{Re}_K) \left(\mathbf{u} \nabla \cdot \mathbf{N} + \nabla q - \nabla \cdot \left(\frac{1}{\mathrm{Re}} \mathbf{D}(\mathbf{N}) \right) \right) \right) \right] d\Omega_K. \end{aligned} \tag{17}$$

The stabilization parameter $\tau(\mathrm{Re}_K)$ presents in Eq. (17) are designed by Franca *et al.* [26] for $k \geq 2$, given as

$$\begin{aligned} \tau(\mathrm{Re}_K) &= \frac{\xi(\mathrm{Re}_K)}{\sqrt{\lambda_K} |\mathbf{u}|_2}, \\ \mathrm{Re}_K &= \frac{|\mathbf{u}|_2}{4\sqrt{\lambda_K} \eta(\dot{\gamma}) / \rho} \text{ and } |\mathbf{u}|_2 = \left(\sum_{i=1}^{2} |u_i|^2 \right)^{1/2}, \\ \xi(\mathrm{Re}_K) &= \begin{cases} \mathrm{Re}_K, 0 \leq \mathrm{Re}_K < 1 \\ 1, \mathrm{Re}_K \geq 1 \end{cases}, \\ \lambda_K \max_{0 \neq \mathbf{N} \in (R_k(\Omega_K)/\sim)^N} &= \frac{\|\Delta \mathbf{N}\|^2_{0,\Omega_K}}{\|\nabla \mathbf{N}\|^2_{0,\Omega_K}}, \Omega_K \in C_h. \end{aligned} \tag{18}$$

The parameter λ_K is evaluated as the largest eigenvalue for the associated eigenvalue problem defined for each Ω_K following the one that has been computed by Harari *et al.* in [27] for quadratic triangular element. The appropriate trial solutions for $\mathbf{u}$ and p within an element, $e_i, i = 1, 2, 3, ... N_e$ are discretized in Eqs. (17) and (18) as follow,

$$\begin{aligned} \mathbf{u} &= \mathbf{u}^{e_i} = \mathbf{N}_j^{e_i} \mathbf{u}_j, \\ p &= p^{e_i} = q_j^{e_i} p_j, \end{aligned} \tag{19}$$

where $j = 1, 2, 3, 4, 5, 6$ corresponding to three corner nodes and three mid-side nodes per element e_i. To linearize the non-linear terms that are existed in the dependent variables of the advection terms in Navier-Stokes equations, help from an iterative method is needed here. For that purpose,

the Newton-Raphson method is being implemented to linearize the non-linear systems of equations presented in Eq. (17). Hence, Eq. (17) need to be written in terms of its residual function, $\mathbf{R(U)}$ as

$$\mathbf{R}(\mathbf{U}) = \left[\mathbf{K}(\mathbf{U})\right]\mathbf{U} - \left\{\mathbf{F}\right\} = 0, \tag{20}$$

where $\mathbf{U}$ is defined as the vector for the degrees of freedom for variables $\mathbf{u}_h$ and p_h, $\left[\mathbf{K}(\mathbf{U})\right]$ stands for the stiffness matrices and $\left\{\mathbf{F}\right\}$ denotes the force vector. The convergence analysis performed in this study is converged at 10^{-6} where the convergence criteria, τ for the maximum residual norm, R_I are calculated as

$$\tau \le \sqrt{\sum_{I=1}^{N} R_I^2}. \tag{21}$$

Hence, according to the Newton-Raphson method, the solutions for the degrees of freedom are found as

$$\mathbf{U}^{b+1} = \mathbf{U}^b - \mathbf{J}^{-1}(\mathbf{U}^b)\mathbf{R}(\mathbf{U}^b), \tag{22}$$

where b acts as the iteration and $\mathbf{J} = \partial\mathbf{R} / \partial\mathbf{U}$ indicates the Jacobian matrix. Meanwhile, The Jacobian matrix of six quadrature points is adopted in this study to approximate the integrals in Eq. (17).
Based on the GLS formulations explained before, to sum up, the following steps summarised the algorithms applied in the developed source code by using the Matlab programming software:

i. The geometry for the computational domain is constructed as in Figure 1 by using the equation stated in Eqs. (7) and (8) where the finite element meshes are generated from a "mesh2d" function developed by Darren Engwirda.
ii. The nodes and their edges are generated. The numbering for the variables defined at each node of the element is performed for the global degree of freedoms $\{u, v, p\}$.
iii. The boundary conditions, convergence tolerance τ and all related parameters are prescribed. The Stokes solution for the Newtonian fluid flow is solved as the initial guess for $\{u, v, p\}$.
iv. The element matrix for each finite element is approximated. The integrals are computed by using a Gaussian quadrature rule with the stabilization GLS terms calculated according to Eq. (18).
v. The element matrices are being assembled forming a global matrix and is solved subjected to the boundary conditions imposed as stated in Eq. (13).
vi. The residual functional, $\mathbf{R(U)}$ in Eq. (20) is computed.
vii. The convergence tolerance, τ that is defined in Eq. (21) is calculated for the convergence analysis of the solution. If the condition is fulfilled, the iteration will stop and the solutions are obtained at the previous step.
viii. If the previous condition is not obeyed, the Jacobian matrix $\mathbf{J}$ is evaluated.
ix. The solutions are corrected as $\mathbf{U}^{b+1} = \mathbf{U}^b \delta\mathbf{U}^b$ where $\delta\mathbf{U} = -\mathbf{J}^{-1}(\mathbf{U}^b)\mathbf{R}(\mathbf{U}^b)$.

As the solution for the degrees of freedom $\{u, v, p\}$ is obtained in the last iteration when the limit stated in step (vii) has been fully satisfied, the iteration then will stop.

3.3 Numerical Validation

Numerical algorithms are developed using Matlab programming software to solve the variational form for the momentum and continuity equations stated in Eq. (17). The validation of the present numerical algorithms is employed with the existing study conducted by Xenos *et al.* [11] for the flow of blood in a straight channel with a bell shaped stenosis subjected to the MHD effects. The mesh dependency test is conducted to ensure that the results computed are independent of the total number of domain elements. The test is based on the axial velocity profile along the vertical centreline at $x = 1$ where a refined mesh is generated along the stenotic region. Five different domain elements have been employed in solving the Newtonian $\left(\mu = 0.0035 \text{kgm}^{-1}\text{s}^{-1}\right)$ MHD flow in a constricted channel without considering the porosity effect at $B_0 = 8\text{T}, K = 0$ and $\text{Re} = 300$ by using 13 quadrature points. Based on the curves plotted in Figure 2, it is quite obvious that starting from Mesh 3 onwards the mesh size has achieved mesh independence since the curves for Mesh 3, Mesh 4 and Mesh 5 overlapped with one another without any significant change being noticed.

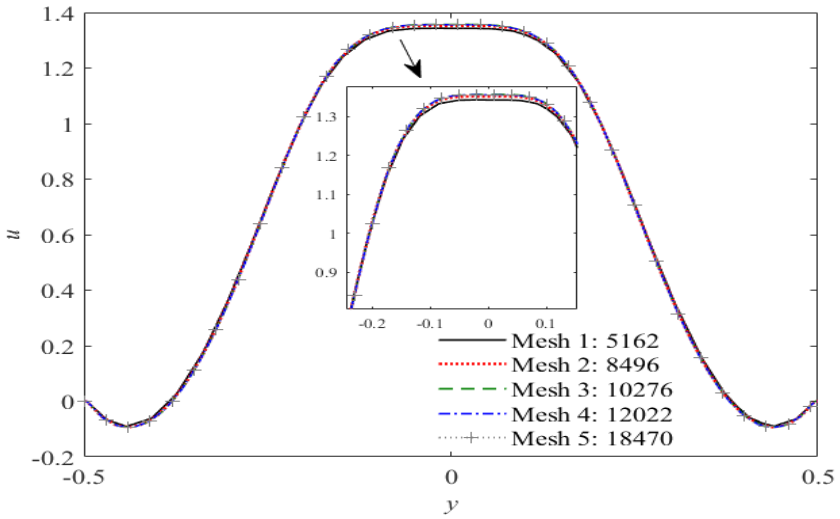

Fig. 2. Mesh independence test for u-velocity profile at $x = 1$ of the channel for $B_0 = 8\text{T}, K = 0$ and $\text{Re} = 300$

Table 1
Comparison of results on the maximum u-velocity and pressure drop, ∇p at various magnetic field strength, B_0

	Results for:	Present study	Xenos *et al.* [11]
$B_0 = 0\text{T}$	Maximum u-velocity	1.5373	1.536
	Pressure drop, ∇p	0.795042	0.8
$B_0 = 8\text{T}$	Maximum u-velocity	1.5108	1.5243
	Pressure drop, ∇p	0.896134	0.9

Hence, Mesh 3 which contained a total of 10276 domain elements is sufficient for the numerical computation of various flow parameters involved in this problem. By using the selected mesh, the

validation of the GLS algorithms is done by comparing the solutions on the maximum u-velocity and pressure drop, ∇p along the straight constricted channel under the influence of an externally applied magnetic field with the existing results [11]. The present results tabulated in Table 1 are computed by using 7 quadrature points since starting from these points the solutions obtained are independent of any change in quadrature points used. The data in Table 1 has proved the efficiency of the developed algorithms through a good agreement on the solutions obtained. In our recent work [28], a similar numerical algorithm on a linear triangular mesh has been verified with similar existing data from [11]. The enhancement of the order of the element to quadratic in this present work has definitely improved the convergence of the solution. Besides, the results on the velocity contour with streamlines pattern obtained from this developed algorithm at varying magnetic field intensity are found in similar form and comparable with [11] as shown in Figure 3.

Overall, it has been confirmed in this section that the GLS algorithms developed here is works effectively and properly. In addition, the accuracy of the solution $\{u,v,p\}$ computed by using the quadratic triangular element is also improved in comparison to my recent findings in [28] that used a linear triangular element as the interpolation function for the dependent variables $\{u,v,p\}$.

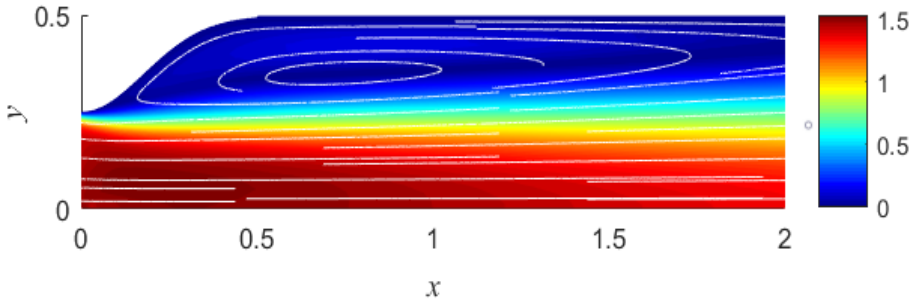

(a) $B_0 = 0\text{T}$

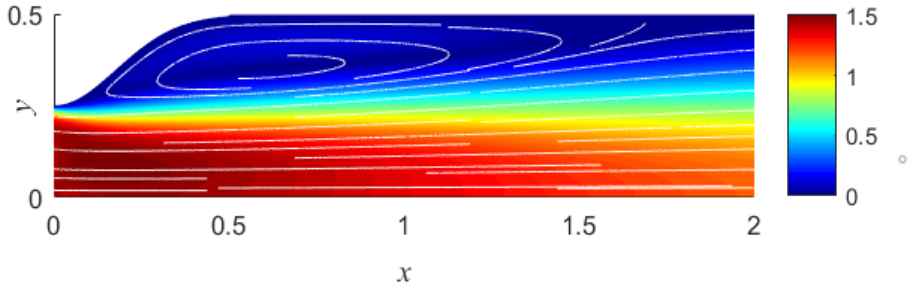

(b) $B_0 = 8\text{T}$

Fig. 3. Velocity contour and streamlines pattern for $\text{Re} = 300$ obtained from the present method at various magnetic field strength applied: (a) $B_0 = 0\text{T}$ (b) $B_0 = 8\text{T}$

3. Result and Discussion

A numerical investigation is carried out with an intention to analyse the effects of physical parameters defining the blood flow behaviour and flow geometry in terms of varying values of maximum height of stenosis, τ_m, Hartmann number, M, and permeability constant, K of the porous medium on the flow characteristics of blood in terms of the distribution of axial velocity and streamline pattern. All the graphical results are plotted by using the following set of parameters taken from [20], [25], [29] and [30]: $a = 0.0075\text{m}$, $l_0 = 0.015\text{m}$, $d = 0.005\text{m}$, $x_{\max} = 0.06\text{m}$, $x_1 = 0.025\text{m}$,

$q = 0.0002\text{m}$, $\rho = 1050\text{kgm}^{-3}$, $\mu = 0.00345\text{kgm}^{-1}\text{s}^{-1}$, $\beta = 30^{\circ}$, $r_1 = 0.51a$, $h = 2a$, $\sigma = 0.8\text{S/m}$ and $\text{Re} = 300$. The Reynolds number, Re is fixed at $\text{Re} = 300$ throughout the numerical analysis, since varying the values of M and K are the main interests in this study. The values assigned for parameter M are dependent on the reference magnetic flux intensity, B_0 which is applied perpendicularly to the direction of blood flow in Tesla (T) unit. The values assigned for M are 0,2 and 4 corresponding to the respective values for B_0 equivalent to 0T, 8.755950T and.17.511901T calculated from Eq. (12) by considering $\bar{u}_r = 6.571429 \times 10^{-2}\,\text{ms}^{-1}$. The mesh independence test is performed to the computational domain involved in this present study prior to further investigation of the numerical simulations of blood flow characteristics. The test is evaluated at several locations along the bifurcated channel for five different domain elements. The u-velocity profiles displayed in Figure 4 are computed at two different locations of $x = 0.6667$ and $x = 3.6$ which are located at the first throat of an overlapping stenosis and the daughter branch, respectively. The results for the axial velocities plotted in this figure are generated by using 9556, 13124, 16138, 19736 and 33636 domain elements. From Figure 4 (a), it is clearly seen that no significant change is spotted between each curve generated from these five varying numbers of domain elements. However, in Figure 4 (b), the curve plotted for Mesh 1 was noticed to have deviated from the other curves (Mesh 2, Mesh 3, Mesh 4 and Mesh 5). The results on u-velocity profiles for Mesh 2, Mesh 3, Mesh 4 and Mesh 5 look similar and overlapped with one another, hence showing that the mesh sizes have achieved the mesh independence starting from Mesh 2.

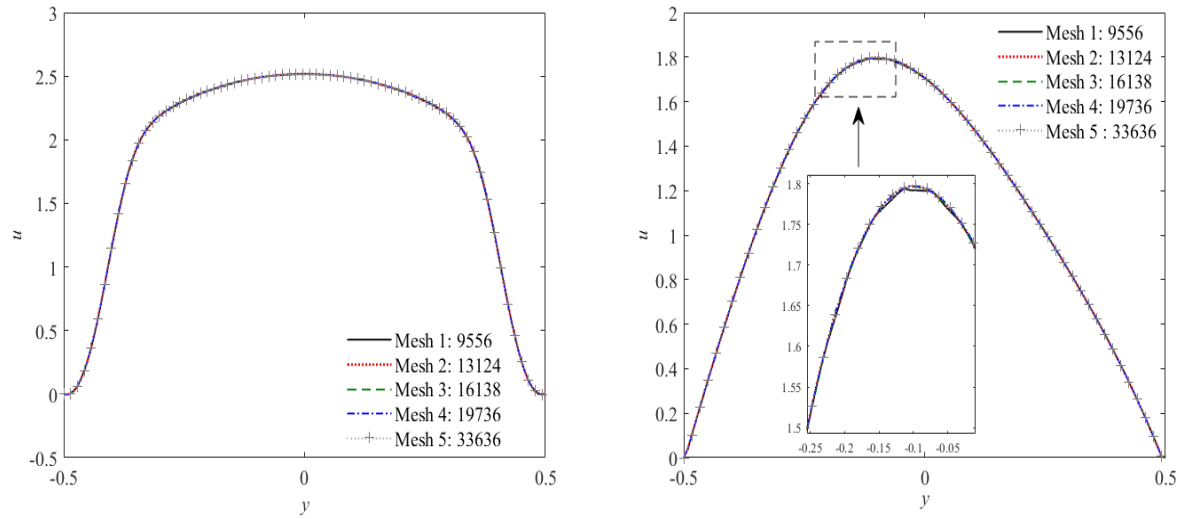

(a) $x = 0.6667$ (b) $x = 3.6$

Fig. 4. Mesh independence test computed for u-velocity profile of the stenosed bifurcated channel for $\text{Re} = 300,\ M = 2, K = 0.3$ and $\tau_m = 0.3a$ at: (a) $x = 0.6667$ (b) $x = 3.6$

Due to that, the numerical computation involves in this study for $\tau_m = 0.3a$ is computed by using Mesh 2 containing 13124 domain elements as shown in Figure 5 (c). Consequently, as visualized in Figure 5, a number of domain elements that are needed to obtain a satisfactory solution for $\tau_m = 0a$, $\tau_m = 0.2a$ and $\tau_m = 0.4a$ are 13614, 13545 and 12856, respectively.

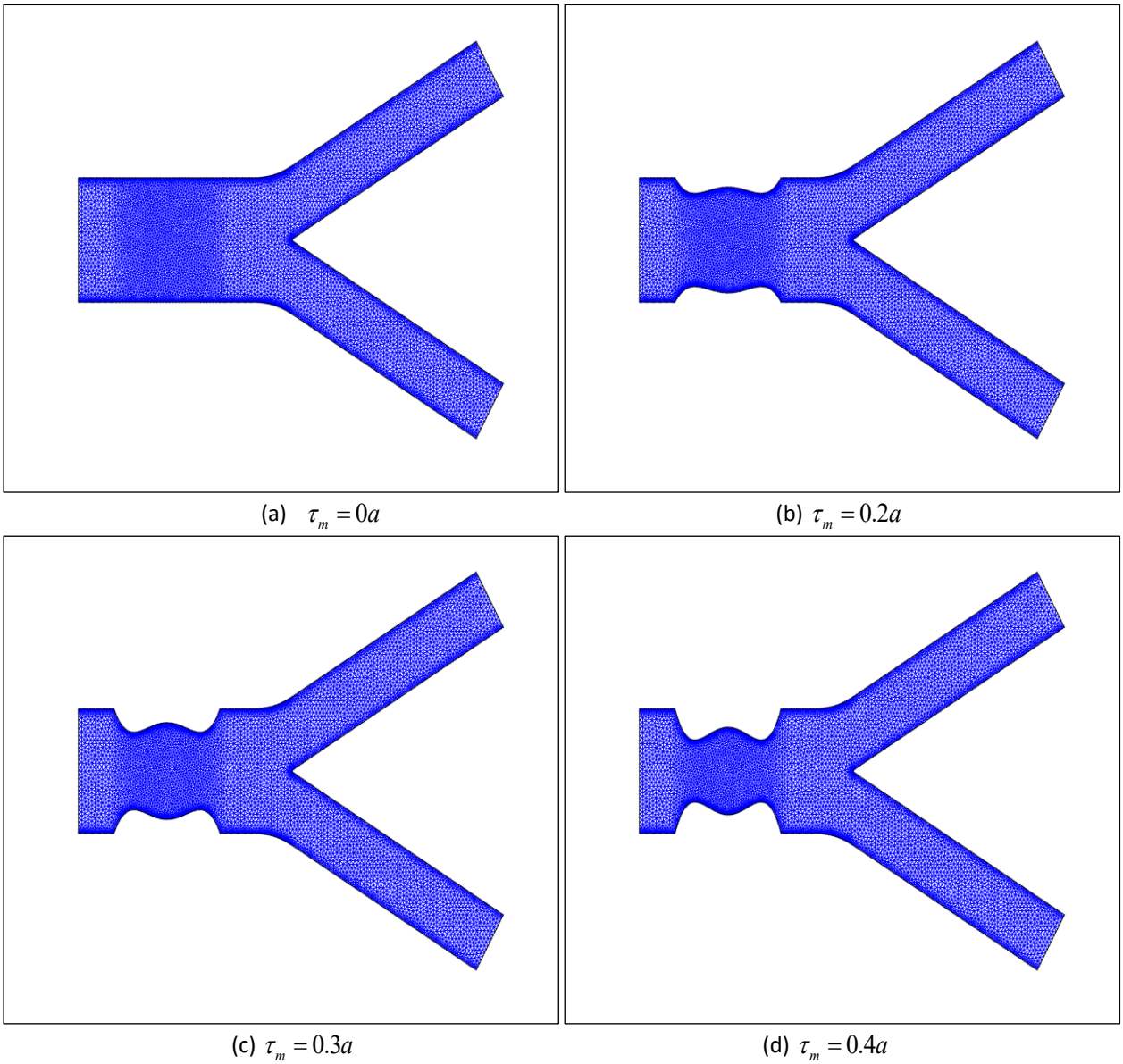

Fig. 5. The selected mesh for different height of stenosis, τ_m : (a) $\tau_m = 0a$ (b) $\tau_m = 0.2a$ (c) $\tau_m = 0.3a$ (d) $\tau_m = 0.4a$

Figure 6 illustrates the influence of varying size of maximum height of stenosis, τ_m on the dimensionless axial velocity profiles across the second throat of overlapping stenosis region located at $x = 1.$ The curves are distributed in an almost similar pattern where the velocity is decreasing from its maximum value with an increase in the direction of magnitude $y,$ corresponding to a parabolic velocity profile imposed at the inlet and non-slip condition employed along the vessel wall. As the severity of stenosis gets enlarged, the axial velocity increases reaching a finite value of the maximum velocity at the axis of symmetry. A reverse trend is observed near the arterial wall for an increase in the maximum height of stenosis which is triggered by the formation of reverse flow in the downstream region of stenosis.

The influence of various permeability constant, K on the axial velocity profiles are plotted along the apex of the bifurcated artery as shown in Figure 7. All of the curves plotted are distributed in an identical pattern where the curves are increasing up to a certain region in the middle axis of the daughter branch before they decrease to zero at the apex of the branch artery. The influence of the

permeability constant, K on axial velocity distributions of blood is not obviously seen in comparison to the previous figure. The velocity is slightly enhanced with an increase in permeability of the porous medium which is in similar agreement with findings from [5] and [7].

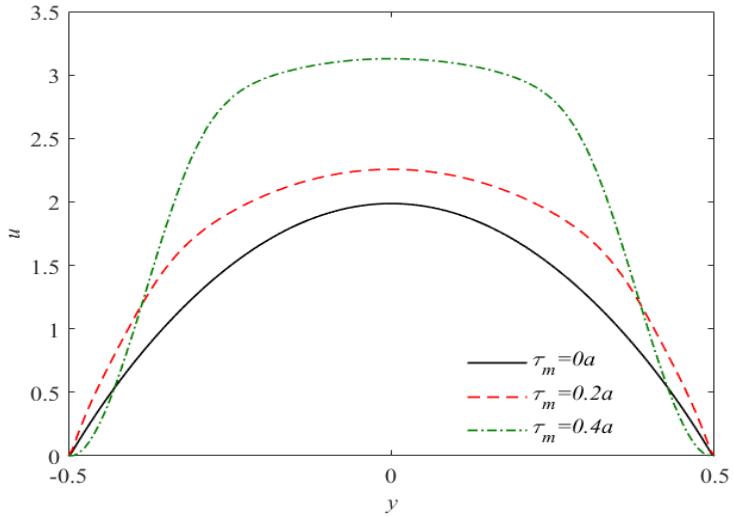

Fig. 6. Effect of stenosis height, τ_m on axial velocity, u at $x=1$ (throat of stenosis)

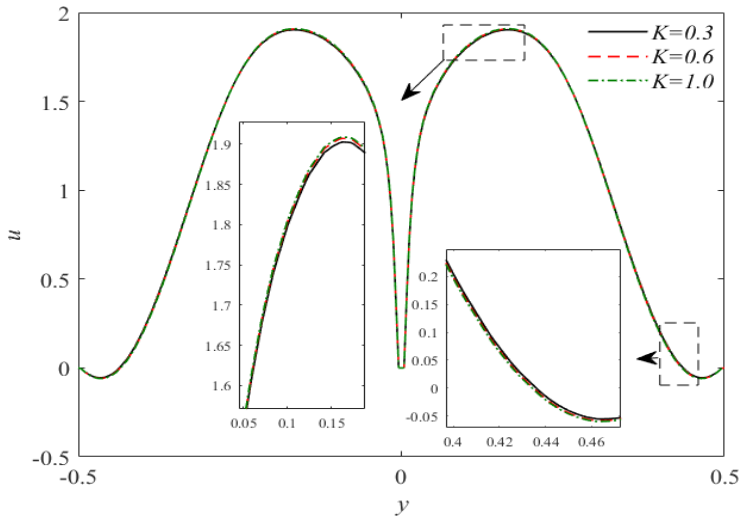

Fig. 7. Effect of permeability constant, K on axial velocity, u at $x=2.0118$ (apex)

Figure 8 on the other hand reveals the behaviour of the streaming blood when subjected to the increasing strength of magnetic field intensity applied in terms of the curves plotted for velocity versus Hartmann number, M. The results presented in this figure are plotted for the flow velocity across the upper daughter branch at the axial position of $x=3.6$. The production of Lorentz force through an interaction between the magnetic flux intensity, B_0 applied and an induced electric current has a tendency to oppose the fluid motion. Due to that, an increment in the magnetic flux strength, B_0 applies indicated by the rise in Hartmann number, M caused the flow velocity of blood to reduce, as can be seen in Figure 12. The graph pattern for all sets of Hartmann numbers, M is skewed to the left side (inner wall) of the daughter branch resulting from the development of the

recirculation zone on the outer arterial wall indicated by a reverse trend of flow velocity near the outer arterial wall. The effects of these physical parameters $(\tau_m, M \text{ and } K)$ are then being investigated and discussed on the changing sizes of vortex that formed around the critical height of stenosis and downstream site of stenosis region which is usually happened in a vessel with overlapping shaped stenosis as portrayed in Figures 9-11 for $\mathrm{Re} = 300$.

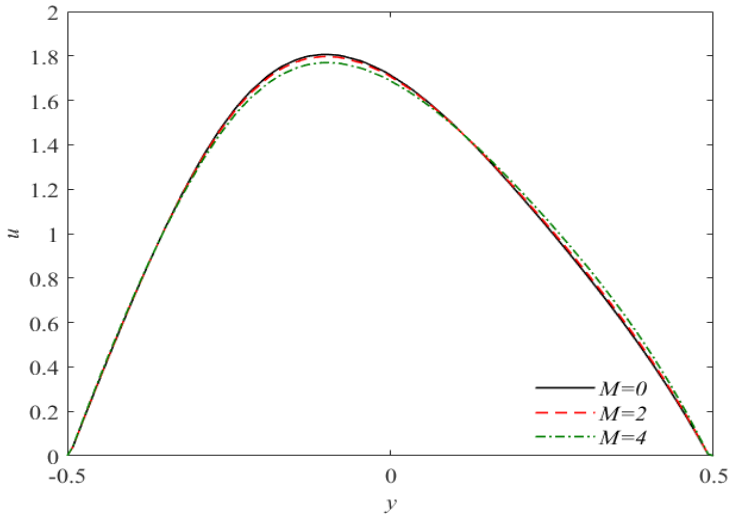

Fig. 8. Effect of Hartmann number, M on axial velocity, u at $x = 3.6$ (upper branch)

The growth in stenosis height, τ_m has a considerable influence on the development of the recirculation area as obviously seen in Figure 9. As the stenosis height increases from $\tau_m = 0.2a$ to $\tau_m = 0.4a$, the length of the vortex that developed along the outer arterial wall also become lengthened. In addition, as the occlusion of the artery gets larger, a noticeable vortex is formed at the critical height of stenosis. Meanwhile, the permeability constant, K has the least effect on the streamlining pattern of the streaming blood as the length of the vortex formed with varying values of permeability constant, K is quite indistinguishable on either the vortex formed at the stenotic or downstream of the stenotic region as shown in Figure 10.

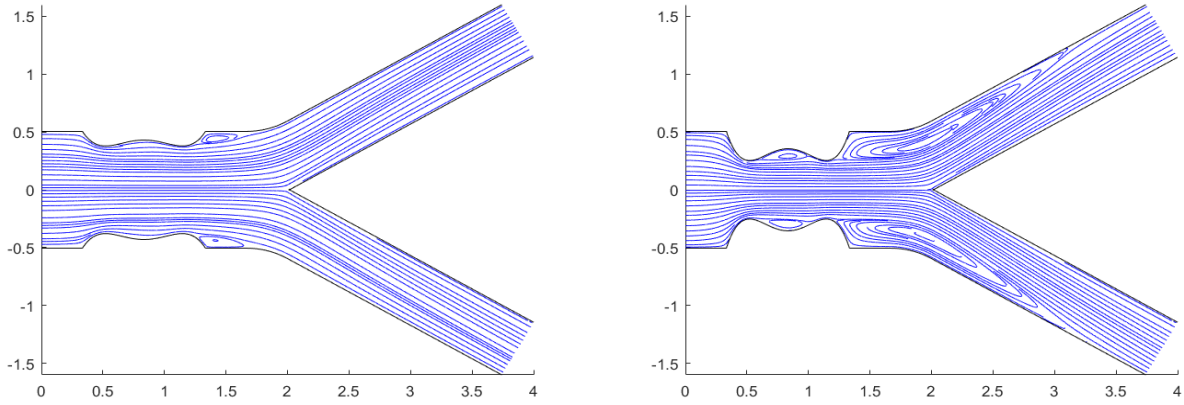

(a) $\tau_m = 0.2a$ (b) $\tau_m = 0.4a$

Fig. 9. Effect of stenosis height, τ_m on streamline pattern for $M = 2$ and $K = 0.3$

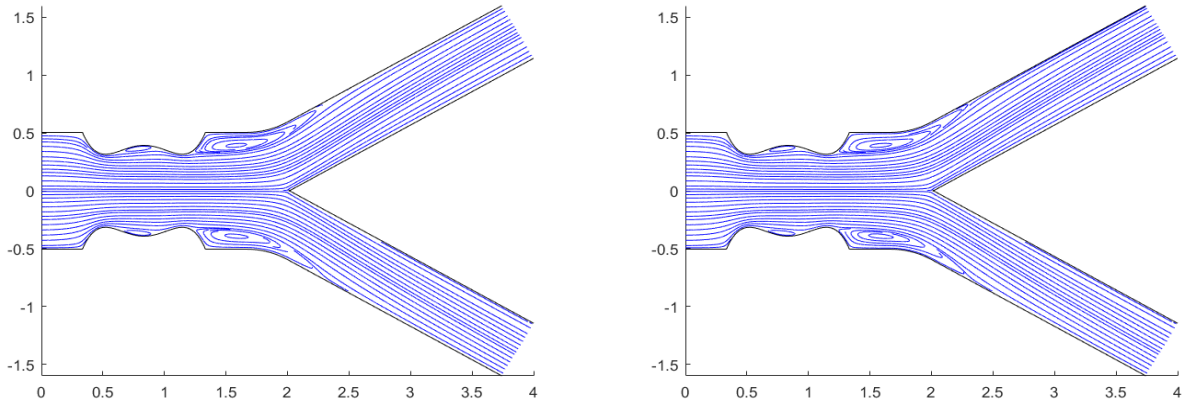

(a) $K = 0.3$ (b) $K = 1.0$

Fig. 10. Effect of permeability constant, K on streamline pattern for $M = 2$ and $\tau_m = 0.3a$

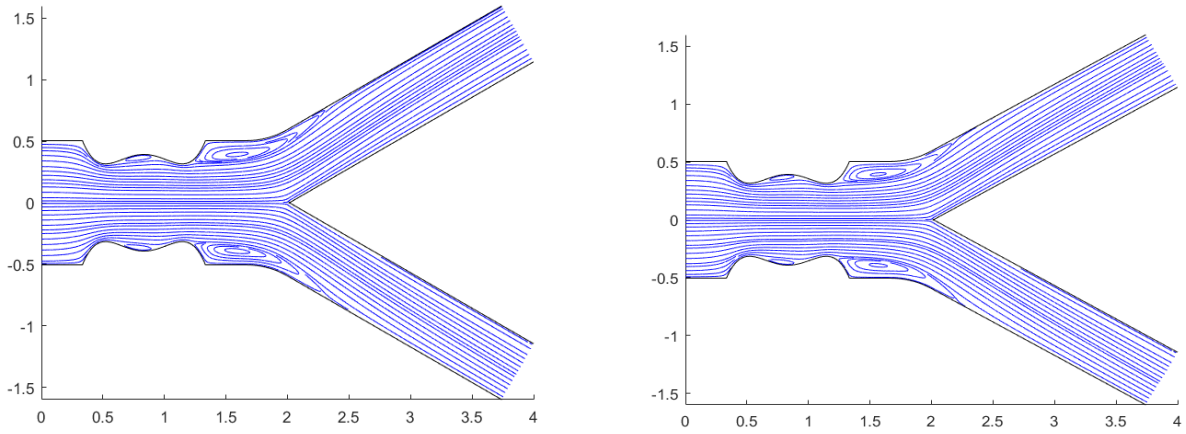

(a) $M = 0$ (b) $M = 4$

Fig. 11. Effect of Hartmann number, M on streamline pattern for $\tau_m = 0.3a$ and $K = 0.3$

Based on the streamline pattern visualized in Figure 11, by increasing the strength of magnetic field intensity applied perpendicularly to the direction of the streaming blood, the length of the recirculation area developed downstream of the stenotic region has also reduced.

4. Conclusions

The hemodynamic of an incompressible Newtonian flow of blood through a porous stenosed bifurcated artery having overlapping shaped stenosis at the parent's artery has been studied concerning the application of an externally applied magnetic field. In this study, observations have been made on the varying effects in stenosis height, τ_m, permeability parameter, K as well as the Hartmann number, M on the flow velocity and streamlining pattern of blood. Based on the validated results that have been presented in the preceding section, the GLS algorithms developed in this current study have been proven as works effectively in solving an incompressible flow of blood under the porosity and magnetic field effects.

1. The growth in stenosis height increases the size of vortex formation considerably and enhanced significantly the axial velocity near the axis of symmetry as it moves away from the arterial wall. This might be due to the sudden change of arterial radii that has accelerated the blood flow at the centre of the vessel.
2. The opposite effect is discovered when the Hartmann number is included as the axial velocity and vortex sizes are decreased. The findings might be of significant interest to surgeons who want to keep patients' blood flow rate at a certain level during the surgical procedure as well as to be used in magnetic therapy of hypertension treatment.
3. A slight enhancement in the axial velocity profiles is observed as the porosity constant is being amplified. Hence for medical purposes, the permeability parameter could be adjusted to the desired level to regulate the higher amount of blood flow rates passing through the blood vessel.

The estimated results presented here may be beneficial to haematologists, biomedical engineers, clinicians and surgeons for regulating the blood flow rate during the entire surgical procedure by applying an appropriate strength of the magnetic field. Despite that, further investigations on the implications of these parameters $(\tau_m, M$ and $K)$ to the other haemodynamic blood flow behaviours are another concern in our next study.

For future study, a thorough investigation of various flow parameters including the wall shear stress, pressure drop and heat transfer parameters should be taken into consideration, so that the real physiological connection of the flow behaviours with biological facts during the therapeutic procedure of electromagnetic hyperthermia in cancer tumour treatment is understandable. Besides, blood rheology as a shear-dependent viscosity must be included for a realistic representation of red cell characteristics.

Acknowledgement
The authors would like to acknowledge the financial support from the Ministry of Higher Education under the Fundamental Research Grant Scheme (FRGS) (FRGS/1/2019/STG06/UTM/02/21) and the Research Management Centre, Universiti Teknologi Malaysia under UTM Fundamental Research (UTMFR) (Q.J130000.2554.21H48) and UTMShine (UTMShine) (Q.J130000.2454.09G88).

References

[1] Nandal, J., S. Kumari, and R. Rathee. "The effect of slip velocity on unsteady peristalsis MHD blood flow through a constricted artery experiencing body acceleration." *International Journal of Applied Mechanics and Engineering* 24, no. 3 (2019). https://doi.org/10.2478/ijame-2019-0040

[2] Srivastava, Neetu. "Analysis of flow characteristics of the blood flowing through an inclined tapered porous artery with mild stenosis under the influence of an inclined magnetic field." *Journal of Biophysics* 2014 (2014). https://doi.org/10.1155/2014/797142

[3] Singh, Ram, G. C. Sharma, and M. Jain. "Mathematical modeling of blood flow in a stenosed artery under MHD effect through porous medium." *International Journal of Engineering* 23, no. 3 (2010): 243-252. https://www.ije.ir/article_71866.html

[4] Abubakar, J. U., and A. D. Adeoye. "Effects of radiative heat and magnetic field on blood flow in an inclined tapered stenosed porous artery." *Journal of Taibah University for Science* 14, no. 1 (2020): 77-86. https://doi.org/10.1080/16583655.2019.1701397

[5] Misra, J. C., A. Sinha, and G. C. Shit. "Mathematical modeling of blood flow in a porous vessel having double stenoses in the presence of an external magnetic field." *International Journal of Biomathematics* 4, no. 02 (2011): 207-225. https://doi.org/10.1142/s1793524511001428

[6] Zaman, Akbar, Nasir Ali, and O. Anwar Bég. "Unsteady magnetohydrodynamic blood flow in a porous-saturated overlapping stenotic artery—numerical modeling." *Journal of Mechanics in Medicine and Biology* 16, no. 04 (2016): 1650049. https://doi.org/10.1142/s0219519416500494

[7] Sinha, A., and G. C. Shit. "Modeling of Blood Flow in a Constricted Porous Vessel Under Magnetic Environment: An Analytical Approach." *International Journal of Applied and Computational Mathematics* 1, no. 2 (2015): 219-234. https://doi.org/10.1007/s40819-014-0022-6

[8] Bakheet, Ahmed, Esam A. Alnussaiyri, Zuhaila Ismail, and Norsarahaida Amin. "Blood flow through an inclined stenosed artery." *Applied Mathematical Sciences* 10, no. 5 (2016): 235-254. https://doi.org/10.12988/ams.2016.511701

[9] Srinivasacharya, Darbhasayanam, and Gade Madhava Rao. "Micropolar fluid flow through a stenosed bifurcated artery." *Nonlinear Analysis: Modelling and Control* 22, no. 2 (2017): 147-159. https://doi.org/10.15388/na.2017.2.1

[10] Sankar, Alana R., Sreedhara Rao Gunakala, and Donna MG Comissiong. "Two-layered blood flow through a composite stenosis in the presence of a magnetic field." *International Journal of Application or Innovation in Engineering and Management* 2, no. 12 (2013): 30-41. https://doi.org/10.5539/jmr.v5n4p26

[11] Xenos, M. A., and E. E. Tzirtzilakis. "MHD effects on blood flow in a stenosis." *Advances in Dynamical Systems and Applications* 8, no. 2 (2013): 427-437. https://campus.mst.edu/adsa/contents/v8n2p21.pdf

[12] Varshney, Gaurav, V. Katiyar, and Sushil Kumar. "Effect of magnetic field on the blood flow in artery having multiple stenosis: a numerical study." *International Journal of Engineering, Science and Technology* 2, no. 2 (2010): 967-982. https://doi.org/10.4314/ijest.v2i2.59142

[13] Charkravarty, S., and Subir Sen. "Dynamic response of heat and mass transfer in blood flow through stenosed bifurcated arteries." *Korea-Australia Rheology Journal* 17, no. 2 (2005): 47-62. https://koreascience.kr/article/JAKO200504703989262.page

[14] Weddell, Jared C., JaeHyuk Kwack, P. I. Imoukhuede, and Arif Masud. "Hemodynamic analysis in an idealized artery tree: differences in wall shear stress between Newtonian and non-Newtonian blood models." *PloS one* 10, no. 4 (2015): e0124575. https://doi.org/10.1371/journal.pone.0124575

[15] Jamali, Muhammad Sabaruddin Ahmad, and Zuhaila Ismail. "Simulation of Heat Transfer on blood flow through a stenosed bifurcated artery." *Journal of Advanced Research in Fluid Mechanics and Thermal Sciences* 60, no. 2 (2019): 310-323. https://akademiabaru.com/submit/index.php/arfmts/article/view/2650

[16] Zinani, Flávia Schwarz Franceschini, and Sérgio Luiz Frey. "Galerkin least-squares approximations for flows of Casson fluids through an expansion." In *Brazilian Congress of Thermal Engineering and Sciences (10.: 2004: Rio de Janeiro, RJ).[Proceedings][recurso eletrônico]. Rio de Janeiro: ABCM: UFRJ, 2004.* 2004. http://dx.doi.org/10.5380/reterm.v5i2.61855

[17] Zinani, Flávia, and Sérgio Frey. "Galerkin least-squares finite element approximations for isochoric flows of viscoplastic liquids." (2006): 856-863. https://doi.org/10.1115/1.2201633

[18] Zinani, Flávia, and Sérgio Frey. "Galerkin least-squares solutions for purely viscous flows of shear-thinning fluids and regularized yield stress fluids." *Journal of the Brazilian Society of Mechanical Sciences and Engineering* 29 (2007): 432-443. https://doi.org/10.1590/S1678-58782007000400012

[19] Martins, R. R., F. S. Silveira, and M. L. Martins-Costa. "Numerical investigation of inertia and shear-thinning effects in axisymmetric flows of Carreau fluids by a Galerkin least-squares method." *Latin American applied research* 38, no. 4 (2008): 321-328.

[20] Chakravarty, Santabrata, and Prashanta Kumar Mandal. "An analysis of pulsatile flow in a model aortic bifurcation." *International journal of engineering science* 35, no. 4 (1997): 409-422. https://doi.org/10.1016/S0020-7225(96)00081-X

[21] Luisa Sousa, Catarina F. Castro, Carlos Conceição António, and R. Chaves. "Computational techniques and validation of blood flow simulation." *WSEAS Transactions on Biology and Biomedicine* 8, (2011): 145-155. http://www.wseas.us/e-library/transactions/biology/2011/54-253.pdf

[22] Haghighi A, and Pirhadi N. "A numerical study of heat transfer and flow characteristics of pulsatile blood flow in a tapered artery with a combination of stenosis and aneurysm." *International Journal of Heat and Technology*.37, no.1 (2019): 11–21. https://doi.org/10.18280/ijht.370102

[23] Huh HK, Ha H, and Lee, SJ. "Effect of non-Newtonian viscosity on the fluid-dynamic characteristics in stenotic vessels." *Experiments in Fluids* 56, no. 8 (2015): 1–12. https://doi.org/10.1007/s00348-015-2037-0

[24] Jamalabadi MYA, Daqiqshirazi M, Nasiri H, Safaei MR, and Nguyen TK. "Modeling and analysis of biomagnetic blood Carreau fluid flow through a stenosis artery with magnetic heat transfer: A transient study." *PLoS One* 13, no. 2 (2018): e0192138. https://doi.org/10.1371/journal.pone.0192138

[25] Chakravarty, S., and P. K. Mandal. "Mathematical modelling of blood flow through an overlapping arterial stenosis." *Mathematical and computer modelling* 19, no. 1 (1994): 59-70. https://doi.org/10.1016/0895-7177(94)90116-3

[26] Franca, Leopoldo P., and Sérgio L. Frey. "Stabilized finite element methods: II. The incompressible Navier-Stokes equations." *Computer Methods in Applied Mechanics and Engineering* 99, no. 2-3 (1992): 209-233. https://doi.org/10.1016/0045-7825(92)90041-H

[27] Harari, Isaac, and Thomas JR Hughes. "What are C and h?: Inequalities for the analysis and design of finite element methods." *Computer Methods in Applied Mechanics and Engineering* 97, no. 2 (1992): 157-192. https://doi.org/10.1016/0045-7825(92)90162-d

[28] Zain, Norliza Mohd, Zuhaila Ismail, and Peter Johnston. "A Stabilized Finite Element Formulation of Non-Newtonian Fluid Model of Blood Flow in A Bifurcated Channel with Overlapping Stenosis." *Journal of Advanced Research in Fluid Mechanics and Thermal Sciences* 88, no. 1 (2021): 126-139. https://doi.org/10.37934/arfmts.88.1.126139

[29] Rabby, Mir Golam, Rumia Sultana, Sumaia Parveen Shupti, and Md Mamun Molla. "Laminar blood flow through a model of arterial stenosis with oscillating wall." *International Journal of Fluid Mechanics Research* 41, no. 5 (2014). https://doi.org/10.1615/InterJFluidMechRes.v41.i5.30

[30] Sinha, A., J. C. Misra, and G. C. Shit. "Effect of heat transfer on unsteady MHD flow of blood in a permeable vessel in the presence of non-uniform heat source." *Alexandria Engineering Journal* 55, no. 3 (2016): 2023-2033. https://doi.org/10.1016/j.aej.2016.07.010